INTERPRETATION OF RIO DELL FREEWAY RESPONSE DURING SIX RECORDED EARTHQUAKE EVENTS

K. Romstad, Professor
B. Maroney, Graduate Student
M. Chajes, Graduate Student
Department of Civil Engineering,
University of California, Davis

ABSTRACT

Six earthquakes have been recorded since 1980 on the overpass of Highway 101 at Painter Street in Rio Dell, California, just south of Eureka. Finite element models of the bridge have been constructed and the natural frequency results compared with the recorded motions. Analysis of the experimental data tends to identify the first six modes of vibration. Modeling the backfill-abutment-superstructure interaction is key to the analytical modeling to describe response. Torsional modes of vibration of the individual spans appear heavily influenced by the skew implying use of very simple bridge models should be approached cautiously for such short spans.

INTRODUCTION

Description of Bridge and Instrumentation

The Rio Dell overpass is a two span bridge crossing Highway 101 at Painter Street. The bridge is a monolithic, cast in place, prestressed, concrete, box girder structure with end diaphragm abutments and a two column bent. Both the abutment and bent foundations are supported on piles. The behavior is complicated by a 39° degree skew between the centerline of bent #2 and the centerline of Highway 101 passing beneath and the unbalanced spans of 119 and 146 feet. A strip bearing pad is located at the base of abutment #1 on the west end as part of a designed mechanism to allow for longitudinal movement. The bridge is typical of numerous bridges in California spanning two or four lane separated highways.

The bridge was relatively heavily instrumented in September, 1977 [1,2] and contains twenty strong motion sensors as shown in Figure 1. Channels 12, 13 and 14 measure free field motions (longitudinal, vertical and transverse to the bridge axis respectively) approximately 200 feet northwest of the overpass between the traffic lanes. At the east end of the bridge, triaxial sets of sensors are located both on the embankment (15, 16, 17) and on the end of the bridge deck (9, 10, 11) so that relative motion between the embankment and the deck can be assessed. The west end of the bridge is similarly instrumented except for the absence of a longitudinal sensor on the bridge deck. A triaxial set of sensors (1, 2, 3) is also located at the base of the bent's north column to aid in assessing soil structure interaction. A transverse sensor (7) is located at the base of the deck adjacent to the center bent and vertical sensors are located at midspan of the east (8) and west (6) spans on the north side of the deck. Torsion of the bridge deck cannot be directly assessed since only the north edge of the bridge deck is instrumented.

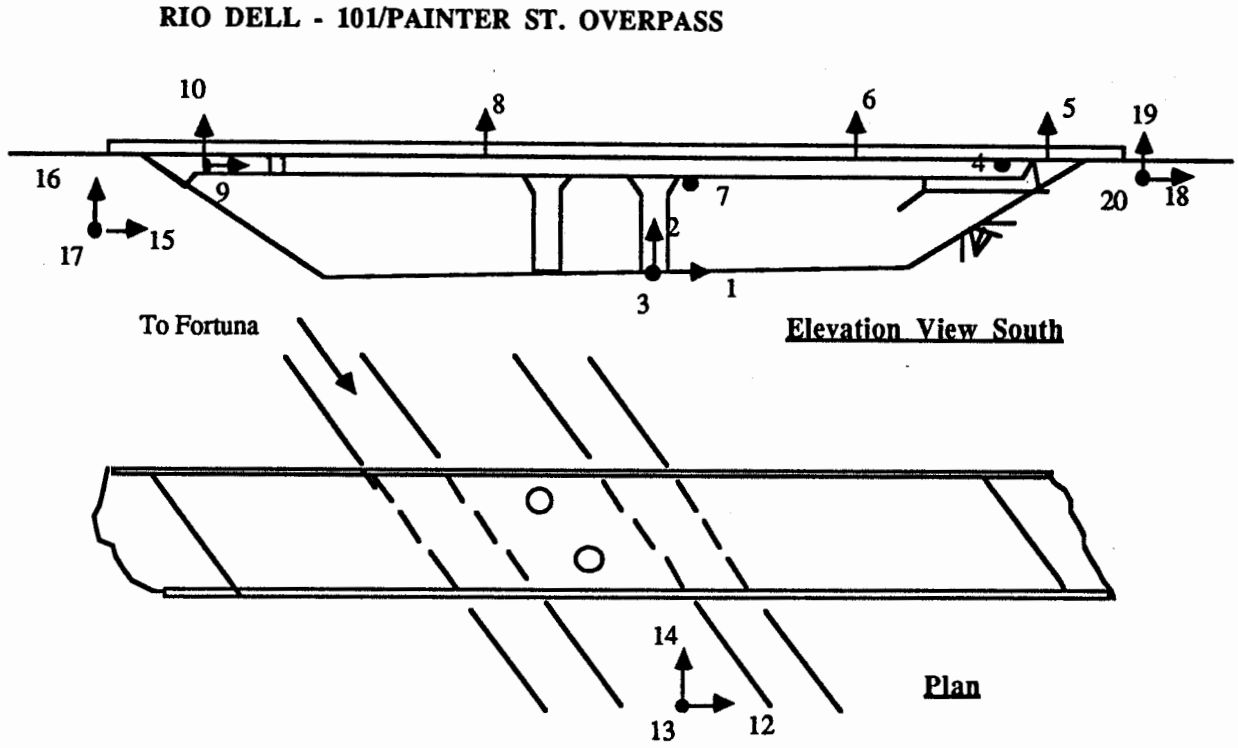

Figure 1 Distribution of Strong Motion Sensors at Painter Street Overpass, Highway 101, Rio Dell, Humbolt County, CA.

Strong Motion Records

Since the overpass was instrumented, it has been shaken by six earthquakes [2] starting with the large (6.9ML) Trinidad offshore earthquake of November 8, 1980 at 72 km from the site. The second earthquake was a smaller (4.4ML) event on December 16, 1982 only 15 km from the site. The other events ranged from 5.1 to 5.5 ML at 27 to 61 km. The six earthquakes are summarized in Table 1. Observation of the free field data in Table 1 shows that the maximum vertical accelerations are less than fifty percent of the maximum transverse accelerations and less than twenty five percent of the maximum longitudinal accelerations. However, the maximum vertical accelerations measured by sensors six and eight on the north end of the deck at the middle of the spans generally equal to or exceed the maximum transverse acceleration measured by sensor 7 of the deck at bent #2. The largest bridge accelerations were caused by caused by the relatively small Rio Dell earthquake of 12/16/82. Unfortunately the free field sensors did not record this event.

TABLE 1

EARTHQUAKES RECORDED BY THE RIO DELL OVERPASS INSTRUMENTATION

Earthquake	Date	Mag. (ML)	Epicent. Distance (km)	Maximum Ground Acceleration C12	C13	C14	Maximum Bridge Acceleration C6	C7	C8
Trinidad	11/08/80	6.9	72	.15g	.03g	.06g	.34g	-	.25g
Rio Dell	12/16/82	4.4	15	-	-	-	.39g	.43g	.59g
Cape Mendocino	08/24/83	5.5	61	-	-	-	.27g	.22g	.16g
Event #1	11/21/86	5.1	32	.46g	.08g	.16g	.24g	.26g	.33g
Event #2	11/21/86	5.1	33	.15g	.02g	.12g	.21g	.36g	.29g
Cape Mendocino	07/31/87	5.5	27	.15g	.04g	.09g	-	.34g	.27g

In Table 2 the complete set of maximum accelerations from all sensors are presented for earthquakes 4, 5 and 6 arranged by direction. These are simply listed here because they contain essentially complete data sets including free field and sensor 7. In each direction the free field motion is given first followed by the base of pier motion. The remaining channels are then listed in sequential order from the west abutment fill to east abutment fill. It is interesting to note the longitudinal accelerations on the abutment fill (15 and 18) and on the structure (11) are essentially the same as the free field motion (12) for all earthquakes. This may indicate the bridge is moving as a rigid body with the ground in the longitudinal direction. In the transverse direction all sensors on the abutment fill (17 and 20) and on the structure (4, 7 and 9) are considerably amplified relative to the free field (14) and base of pier motion (3). All vertical sensors on the fill (16 and 19) and bridge (5, 6, 8 and 10) are amplified relative to the free field (13) and base of pier (2) except sensor 5. This is possibly due to the bearing pad which exist at the base of the abutment.

TABLE 2

MAXIMUM SENSOR ACCELERATIONS FROM EARTHQUAKES 4, 5 AND 6

	Longitudinal Max. Accel. (g/100) Channel					Transverse Max. Accel. (g/100) Channel							Vertical Max. Accel. (g/100) Channel							
Earthquake	12	1	18	11	15	14	3	20	4	7	9	17	13	2	19	5	6	8	10	16
11/21/86*	46	27	45	40	40	16	13	30	23	26	23	23	8	8	18	10	23	33	25	11
11/21/86**	15	11	17	19	17	12	12	25	25	35	30	22	2	5	6	5	20	29	14	4
07/31/87	15	11	20	21	17	9	10	17	18	34	25	26	4	6	19	5	-	26	11	5

Scope of Study

The primary goal of this study is to investigate bridge modeling techniques; particularly relative to the level of sophistication necessary to accurately capture the essential dynamic response characteristics. Emphasis to date has focussed upon the transverse free field motion (C14) which would be expected to induce the largest forces in the bent columns, since the longitudinal motions should be transferred primarily through the deck to the monolithic end walls and into the abutment backfill. The availability of records from six different events of variable magnitudes and originating from several faults over a seven year span should give considerable insight into level of sophistication justified in formulating analytical models.

The primary parameters used to characterize the accuracy of the analytical model are the natural frequencies and modeshapes of the bridge model. If the analytical model of the bridge predicts natural frequencies and mode shapes which agree well with those deduced from the measured motions in the field then it can be expected the stresses and displacements will also be predicted with reasonable accuracy. As a result this study was initially divided into two phases:

1) analysis of the measured field data to deduce the natural frequencies and modeshapes of the "as built" bridge.

2) comparison of analytical models of various levels of complexity with respect to computed differences in natural frequencies and mode shapes, and

Information from the two phases was then compared and calibrated by adjusting abutment springs.

ANALYSIS OF FIELD DATA

A recent paper by Wilson [3] describes the analysis of records obtained on the San Juan Bautista 156/101 Separation Bridge during the 6 August 1979 Coyote Lake event. The amount of actual data for Painter Street is somewhat overwhelming including 109 corrected time history acceleration records and associated Response Spectra and Fourier Amplitude Spectra for the six events. The data has been looked at in a variety of ways and the power spectral density plots will be emphasized herein. Power spectral densities were obtained for individual earthquakes for each sensor both by analyzing the entire time history recorded and by selecting a portion of the record following the last major acceleration pulse when it appeared to approximate free vibration decay.

Figure 2 shows a plot for from earthquake 4 for sensor 8 using both approaches. Both graphs indicate spikes at close to the same points but using the entire record emphasizes the shorter periods (0.14, 0.20) while using the selected interval emphasizes Longer periods (.21, .25, .28). Figures 3 and 4 superimpose functions from the first three earthquakes for sensor 8 using full and partial records and Figure 5 presents the superimposed functions for earthquakes 4, 5 and 6 using the full records. All six earthquakes tend to show a spike at .14-.15 seconds indicating an active natural mode with significant participation of sensor 8. Other spikes tend to be concentrated at about 0.21, 0.25 (smaller) and 0.28-0.30 seconds.

Figure 6 superimposes the power spectral density plots for earthquakes 1, 2, 3, 4 and 5 for sensor 6 located vertically at the center of the west span.. A clearly dominating spike exists between .30 and .32 seconds with smaller spikes at .36 seconds and 0.21 seconds and smaller blips at .16 and .24 seconds. Figure 7 shows a similar plot for sensor 7 and also five earthquakes. Again a dominant mode clearly exists in the 0.28 second range. The smaller spike at about 0.40 seconds is primarily particular to earthquake 2 which recorded the largest accelerations and was nearest to the bridge.

Figure 8 presents a comparison of the average Fourier Amplitude Spectrum for all earthquakes for the transverse motions in the free field (14), at the base of pier (3), on the fill at the top of the east abutment (17), and on the deck (9) adjacent to the east abutment. Note the similarity of the free field and base of pier motions indicating probably only minor soil-structure interaction in this area. Sensors 17 and 9 show considerably amplified motion in the vicinity of 0.28 seconds with the on bridge motion slightly larger than the fill motion. The differences between the free field (14) and the top of abutment motion imply considerable interaction in this area. The similarity of the motions on top of the fill (17, 20) with the motions on the bridge deck (4, 9) adjacent to the abutment are demonstrated in Figure 9. The top of the embankment fill appears to be moving with the bridge deck consistently throughout the events.

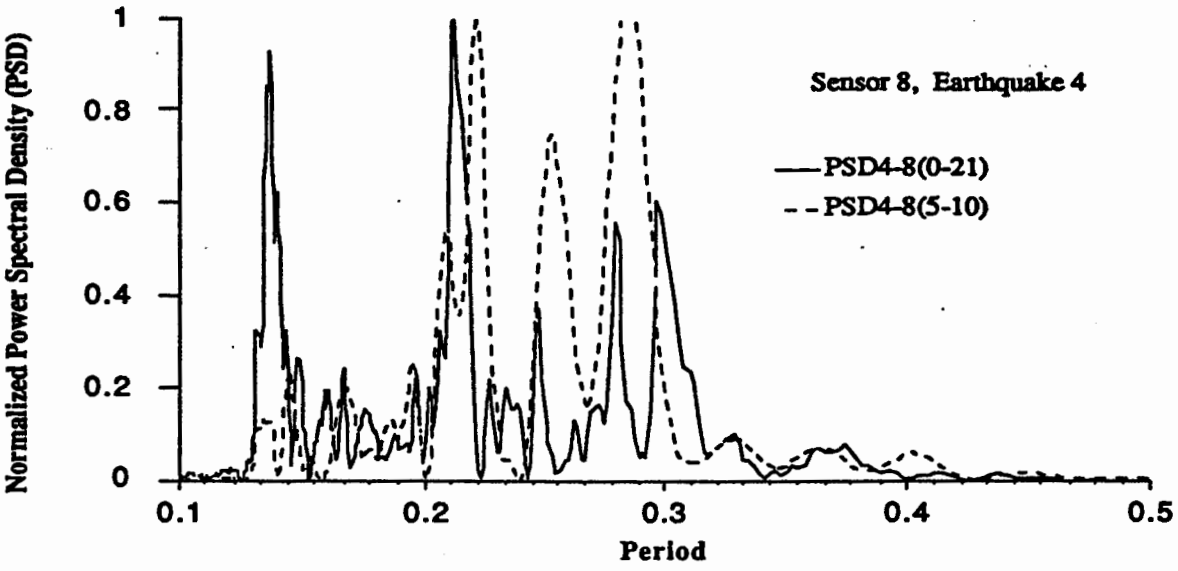

Figure 2 Sensor 8 PSD for Earthquake 4, Two Time Periods

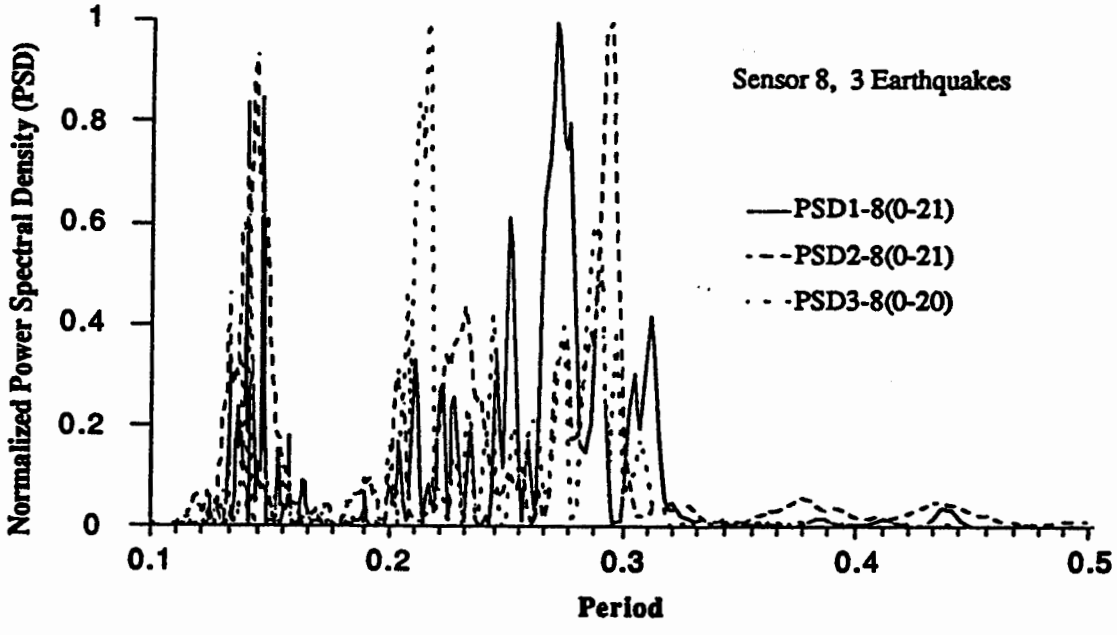

Figure 3 Sensor 8 PSD for Earthquakes 1, 2 and 3, Full Time

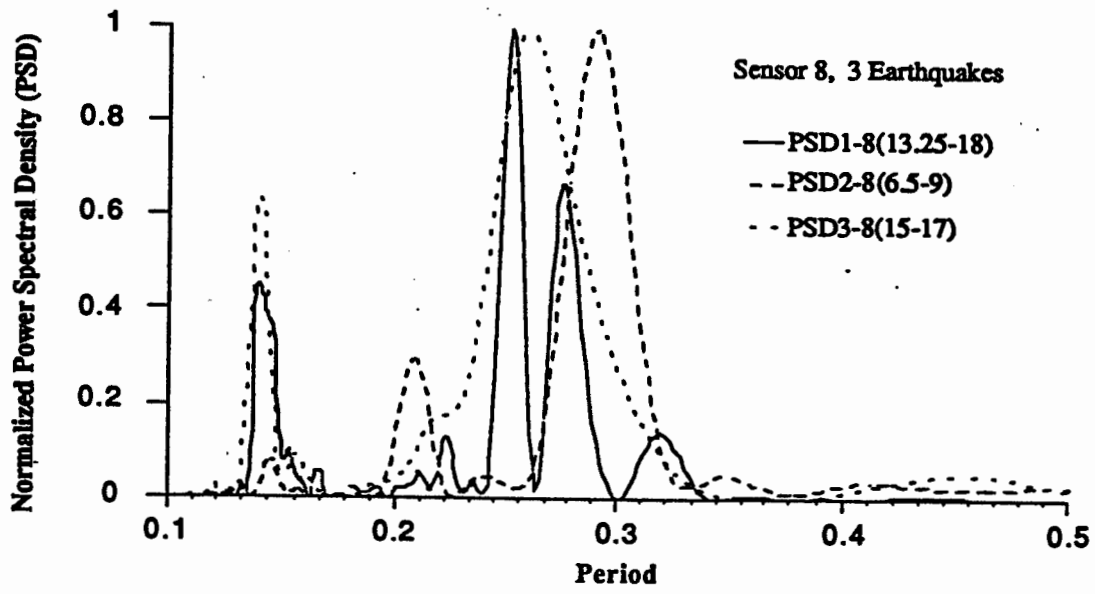

Figure 4 Sensor 8 PSD for Earthquakes 1, 2 and 3, Partial Time

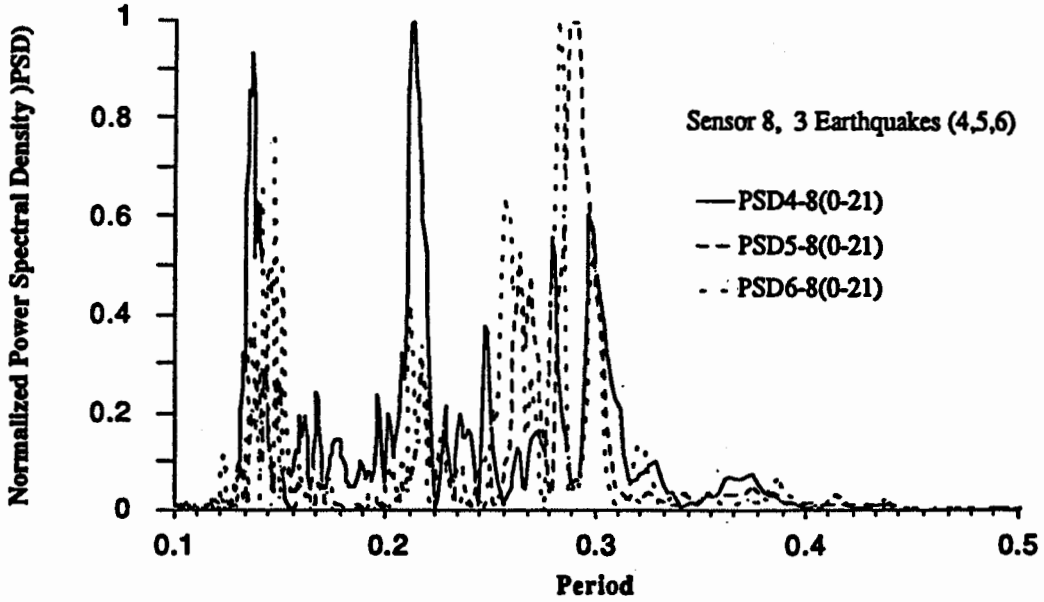

Figure 5 Sensor 8 PSD for Earthquakes 4, 5, and 6, Full Time

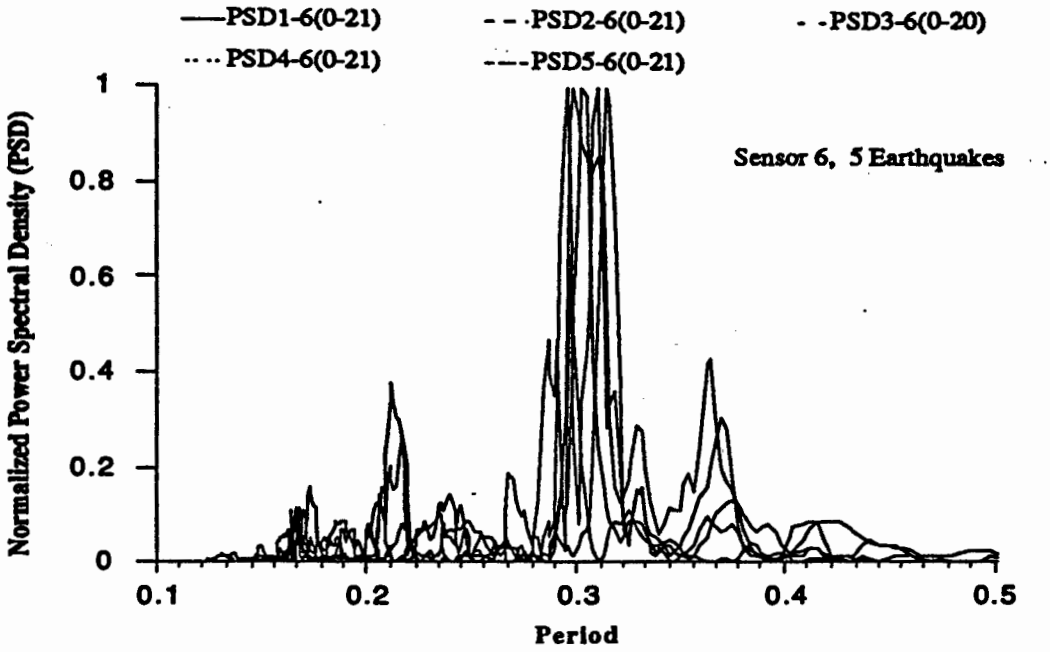

Figure 6 Sensor 6 PSD for Five Earthquakes, Full Time

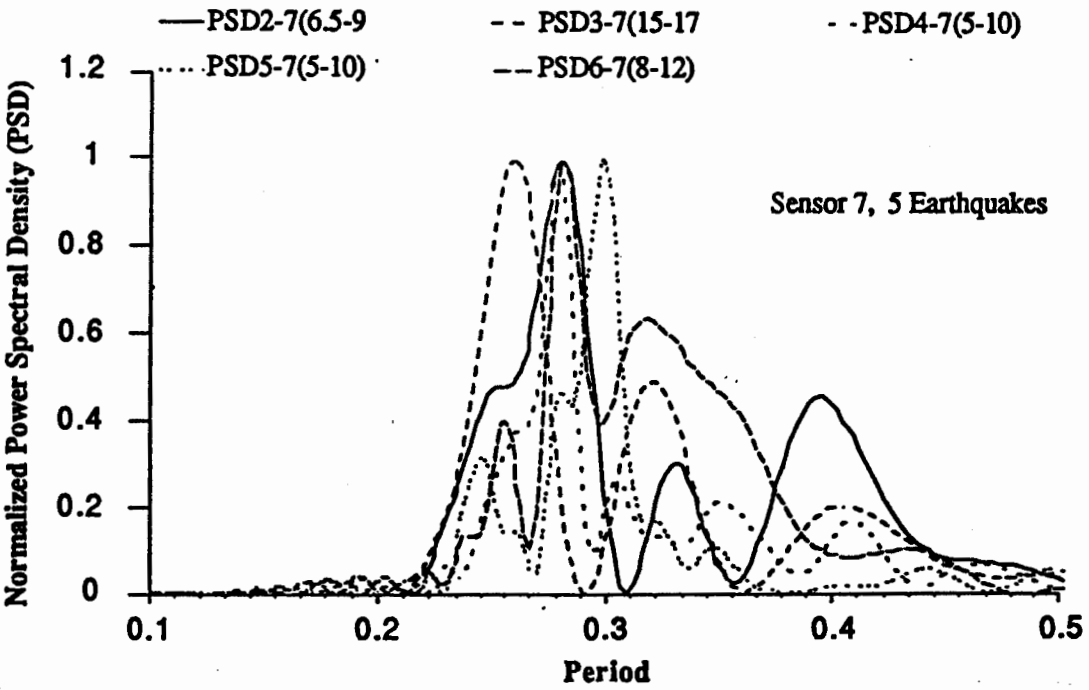

Figure 7 Sensor 7 PSD for Five Earthquakes, Partial Time

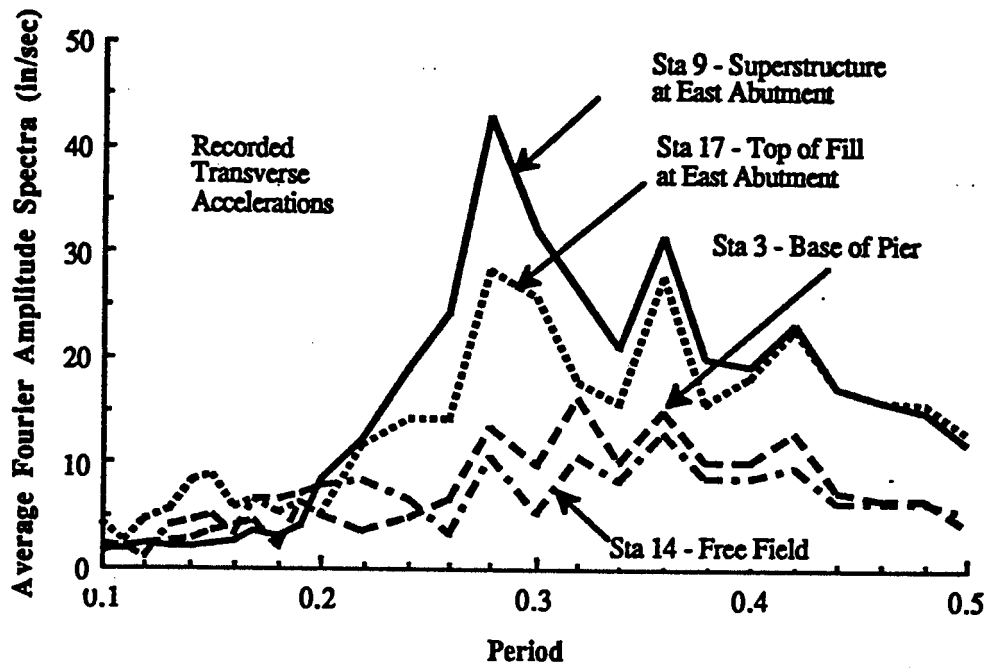

Figure 8 Average Fourier Amplitude Spectrum for 3, 9 and 17

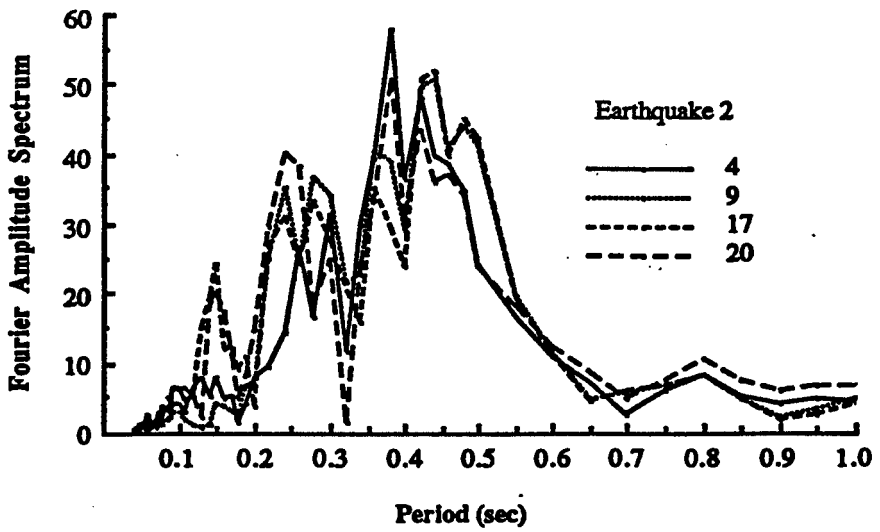

Figure 9 Earthquake 2 Fourier Amplitude Spectrum for 4, 9, 17, 20

ANALYTICAL BRIDGE MODELING

Numerous uncertainties exist in formulating reliable and accurate analytical models to predict the response of concrete bridges to earthquake motions. The Painter Street Overcrossing at Rio Dell is typical of numerous bridges in California which, while apparently simple in form, incorporate most of the uncertainties. The uncertainties investigated included

1) material stiffness modeling of the concrete,

2) finite element model types and mesh size of deck mass and stiffness, and

3) modeling and significance of abutment-backfill and pier foundation-soil interaction springs.

Another major uncertainty present in modeling earthquake response of this type of bridge is estimating the form and magnitude of dissipation of energy (damping) present in the soil foundation superstructure system. We have not yet looked closely at the data to assess energy dissipation or equivalent viscous damping.

Modulus of Elasticity

The modulus of elasticity (E) and shear modulus (G) of the concrete depend upon the actual mix of water, sand, aggregate and cement the contractor used during construction and the age of the concrete. Normally the modulus of elasticity is estimated from the equation

$$E = 33\, w^{1.5} (f_c')^{1/2} \quad (1)$$

where w is the unit weight of the concrete and f_c' is the compressive strength. This is an empirical equation based upon statistical analysis of test data and subject to a local variations. In addition the compressive strength used is normally that specified on the plans and the actual compressive strength found in the field normally exceeds the design strength. In this study we were fortunate to have personnel from the Transportation Laboratory of the State of California take core samples from the bridge and test them in the laboratory. The compressive strength specified on the plans was 3500 psi while the average strength from two laboratory tested core samples was 6400 psi, almost double the design value. The unit weight of the material was measured to be 150 pcf, which gives a modulus of elasticity from equation 1 of 4800 ksi. The actual modulus of elasticity obtained from a stress strain test in the laboratory on one of the core samples was 3800 ksi. This value was used in all subsequent analyses.

Finite Elements Models

A number of finite element models of the Painter Street Bridge were analysized using the computer program STRUDL at the California Department of Transportation Office of Structures computer facilities. The model variations generally differed in the treatment of the stiffness and mass description of the deck and the boundary conditions imposed at the base of the piers and the abutments. Figure 10 illustrates the basic layouts of the two potential models.

The "stick" model in Figure 10 is typical of models used in the dynamic analysis of bridges in California. Using a stick model of the deck means that the torsional, shear, flexural and axial stiffness of the deck are all lumped in a longitudinal one dimensional beam element with six degrees of freedom at each node. This model has the advantage of great simplicity in data preparation and minimal core storage and computation time in the computer. It also permits boundary parameters used to incorporate soil interaction influences. The disadvantages are that rotational inertia effects of the deck about the longitudinal bridge axis, skew and deep beam effects, intermediate diaphragms and deck plate action are not necessarily accurately modeled.

The "grid" model in Figure 10 was chosen to permit the rotational inertia of the deck about the longitudinal axis, skew and deep beam effects and intermediate diaphragms to be directly incorporated and hence serve as an accurate baseline for evaluating the adequacy of the stick model for capturing essential behavior and evaluating a number of the uncertainties present in formulating structural models.

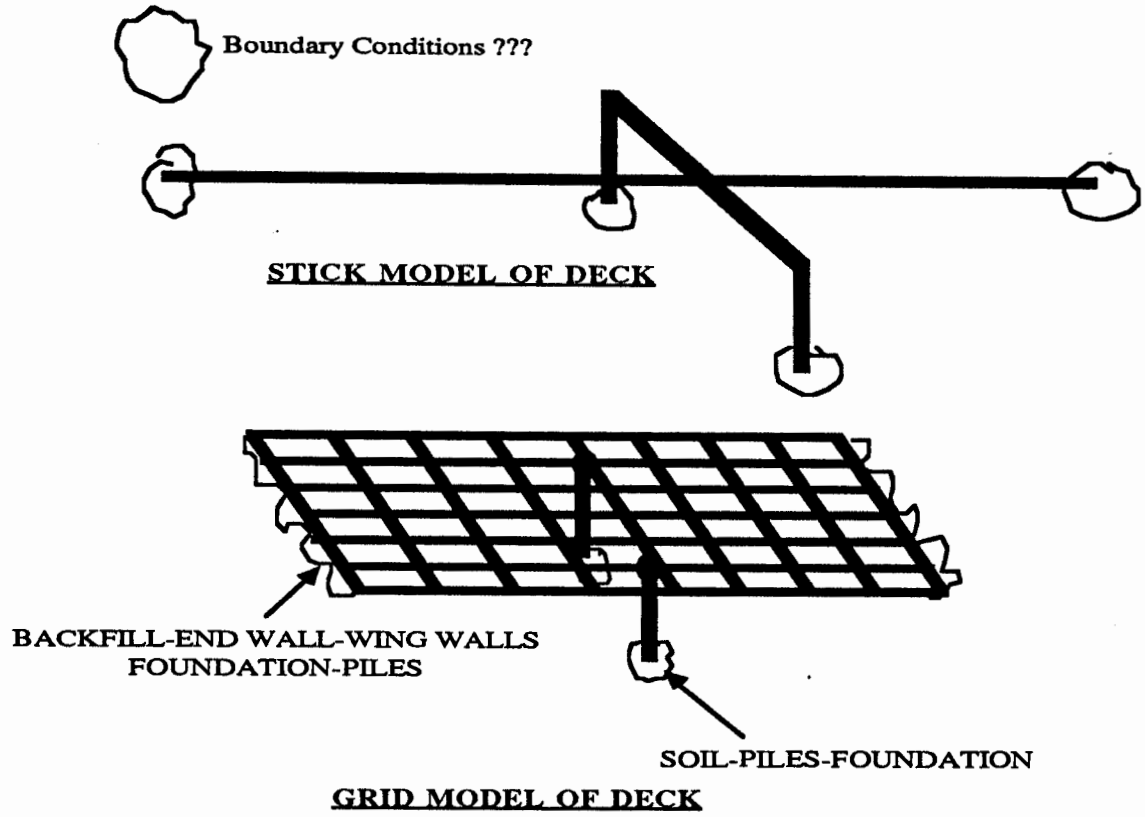

Figure 10 Schematic Finite Element Models of Superstructure

A preprocessor, STRUBAG, used by Caltrans generates STRUDL input coding for the stick model. The finite element model for the finite element grid model had to be laboriously generated point by point. A number of different models for the deck were evaluated in the preliminary analyses in terms of element types, finite element mesh sizes, modeling of the mass variation and choice of cross section properties. The final model for a deck cross section is shown in Figure 3. Each superstructure girder is modeled as a series of longitudinal members with the flanges assumed effective out to one-half the distance to the adjacent girder. The exterior girder elements are assumed to use the entire overhang but not the sidewalk or barrier rail. Transverse diaphragms are also modeled as beams with effective flanges. These properties were then used to determine moment of inertia values for the beams. The web areas were used to determine the effective shear areas and the torsional properties were chosen for the individual beams based upon the torsional stiffness of the entire cross section distributed by tributary area. It was felt the vertical flexural, shear and torsional stiffness of this effectively complicated orthotropic plate would be adequately represented by these beams and their corresponding properties.

A similar model is not adequate for incorporating the transverse stiffness because an intersecting series of beams would not capture the shear stiffness. As a result, plane stress

elements representing the deck were used to fill between the intersecting beams. The element finally selected was the eight node linear strain plane stress element IPQQ in the McDonald-Douglas version of STRUDL. Lower and higher elements were studied and mesh sizes varied to arrive at this selection.

Member section properties were ultimately selected using homogeneous gross sections. It is assumed the sections are only nominally cracked due to shrinkage and temperature because no damage has been observed due to the earthquake. We could find little justification for making more complicated section property calculations.

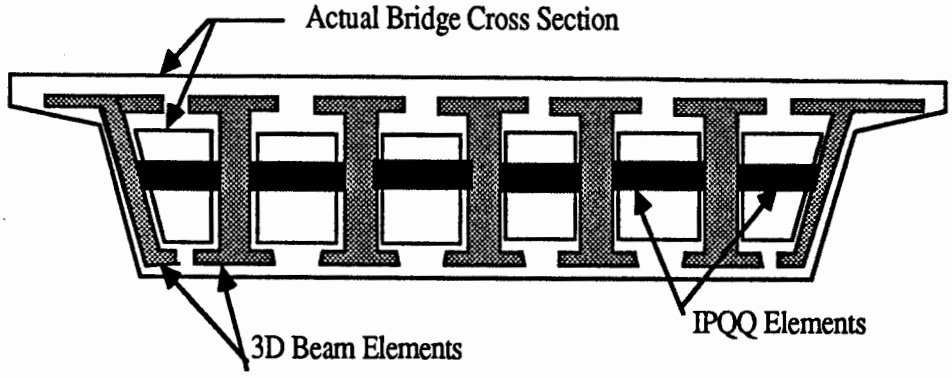

Figure 11 Structural Modeling of Deck in Grid Formulation

Boundary Conditions

Abutment-foundation-backill and pier-foundation interaction springs for use in bridge models have been receiving considerable attention in recent years [5,6,7]. At this point we have not attempted any sophisticated modeling of these interaction influences. In the superstructure we experimented with established spring coefficients for the base of the piers and determined they had little effect on natural frequencies for a range of practical values which tends to be corroborated by the similarity if the measured free field motions with the measured base of pier motions. The most significant boundary condition seems to be clearly the abutment-foundation-backfill condition.

Currently we are assuming the bridge is fixed in all directions at the base of the pier at fixed at the ends of the deck with respect to rotation about all three axes and with respect to translation in the longitudinal and vertical directions. These assumptions, although gross, appear to be reasonable based upon construction conditions and interpretations of the recorded data.

Results

Transverse springs were empirically determined by iteration to yield a computed first transverse period of 0.28 seconds with the relatively sophisticated finite element grid model. Based upon calibrated springs in the transverse direction summing to 39,000 kips/foot the associated first six mode shapes are shown in Figure 12 along with sensor locations. Note that the first vertical mode of 0.36 seconds agrees with the recorded data from sensor 6 while the sixth mode of 0.16 seconds appears to be the mode for by inspecting sensor 8 at about 0.14 seconds. The modes at 0.21 and 0.24 seconds are also visible in the PSD plots for sensors 6 and 8. It appears the finite element model with the calibrated abutment springs in the transverse springs yields a model capable of capturing the essential dynamics of the earthquake response. Much remains to be done!

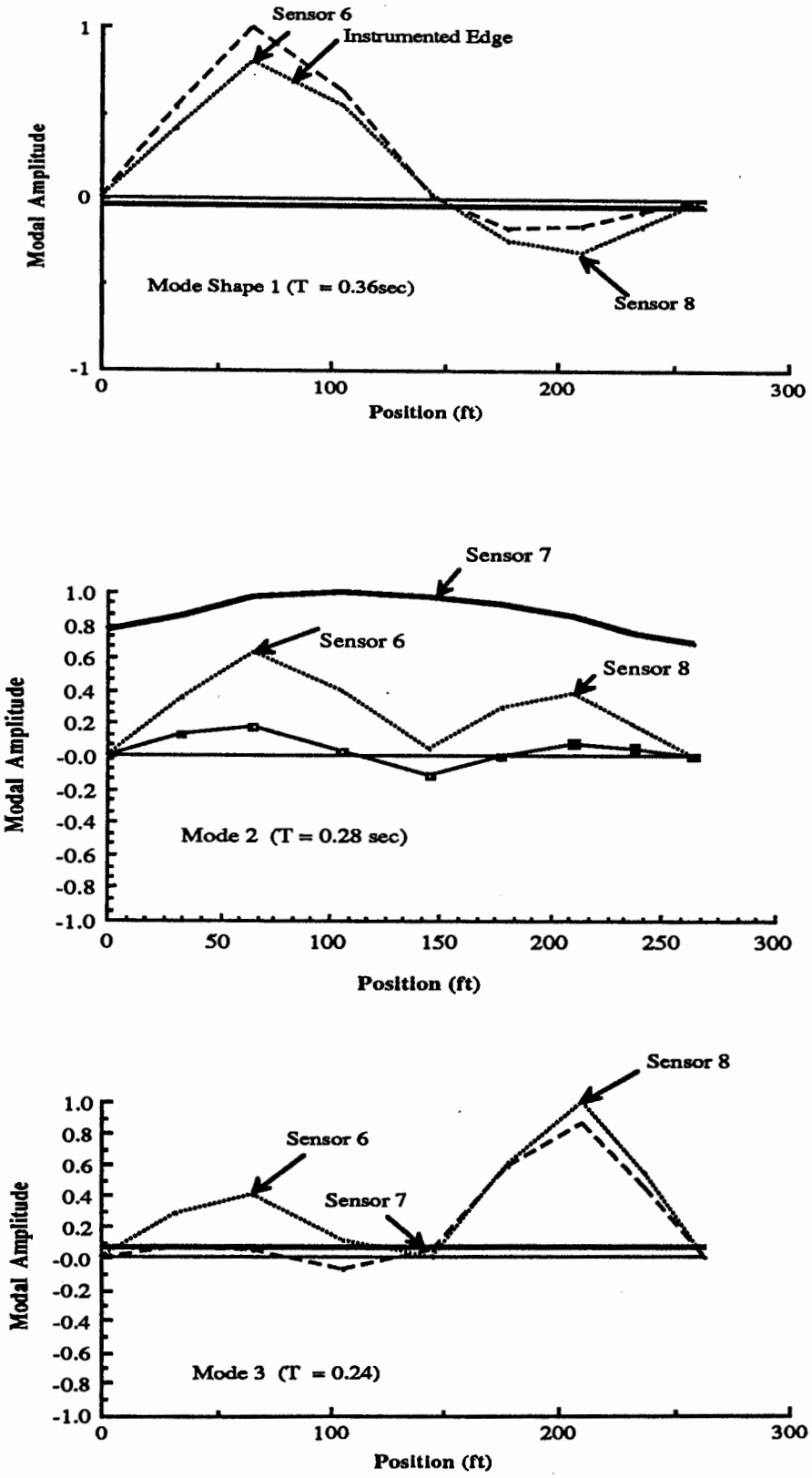

Figure 12 Computed Mode Shapes Using Finite Element Grid Model

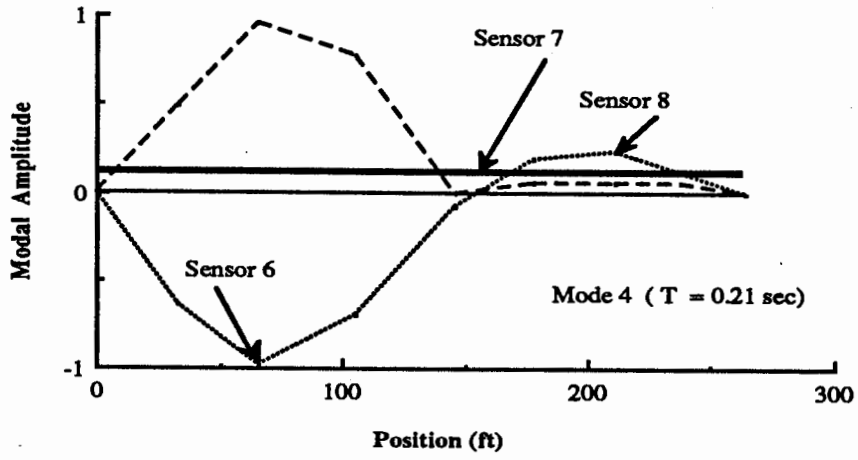

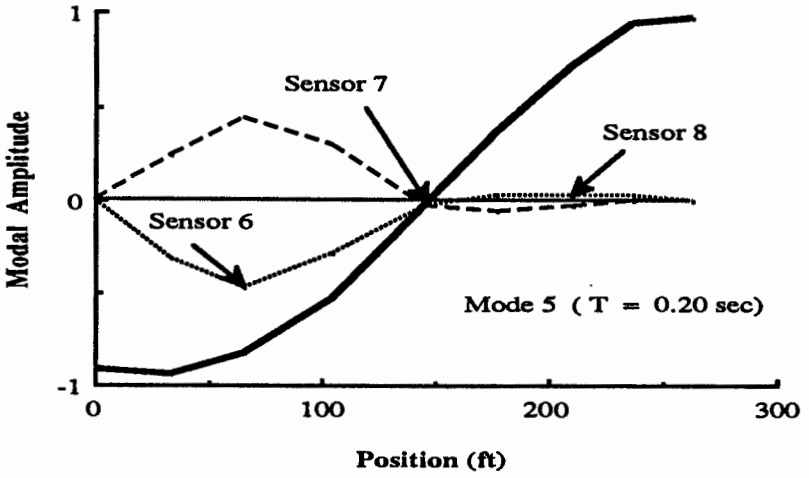

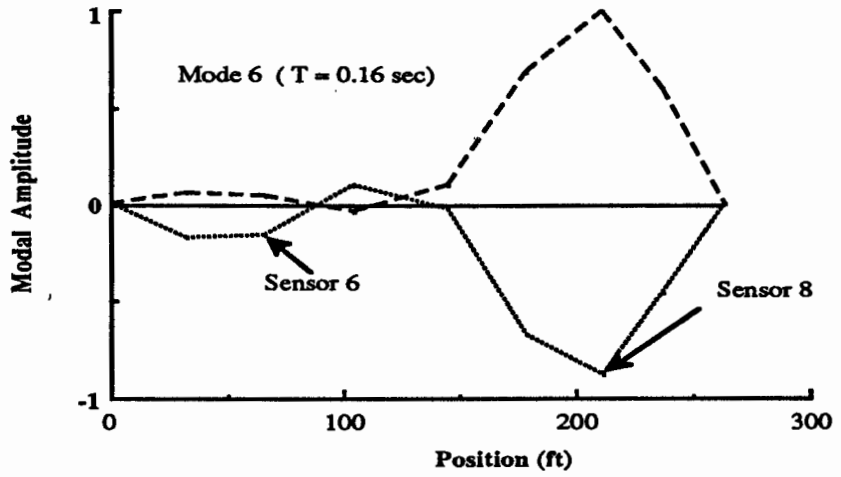

Figure 12 Computed Mode Shapes Using Finite Element Grid Model